Rapid Communications

Fermi surface studies of the low-temperature structure of sodium

S. F. Elatresh,[1,2,*] Mohammad Tomal Hossain,[3] Tushar Bhowmick,[3] A. D. Grockowiak,[4] Weizhao Cai,[3] W. A. Coniglio,[4] Stanley W. Tozer,[4] N. W. Ashcroft,[5] S. A. Bonev,[6,†] Shanti Deemyad,[3,‡] and Roald Hoffmann[2]

[1]*Department of Physics, University of Guelph, Guelph, Ontario, Canada N1G 2W1*

[2]*Department of Chemistry and Chemical Biology, Cornell University, Baker Laboratory, Ithaca, New York 14853-1301, USA*

[3]*Department of Physics and Astronomy, University of Utah, Salt Lake City 84112, Utah*

[4]*National High Magnetic Field Laboratory and Department of Physics, Florida State University, Tallahassee, Florida 32310, USA*

[5]*Laboratory of Atomic and Solid State Physics, Cornell University, Ithaca, New York 14853-1301, USA*

[6]*Lawrence Livermore National Laboratory, Livermore, California 94550, USA*

(Received 19 April 2020; accepted 21 May 2020; published 11 June 2020)

Sodium is the most abundant alkali-metal element and has one of the simplest electronic structures of any metal. At ambient conditions, sodium forms a body-centered-cubic lattice. However, during cooling, it undergoes a partial martensitic phase transition to a complex mixture of rhombohedral polytypes commencing from 36 K. Although the Fermi surface (FS) of bcc sodium has been extensively studied, not much attention has been given to the FS of the martensite structure. Here we report results for the Fermi surface and quantum oscillation (QO) frequencies of several energetically favorable crystal structures of Na at low temperature from first-principles calculations. Interestingly we find that despite drastic differences in the crystal structures of the candidate low-temperature phases of sodium, for all these phases the strongest quantum oscillation peak is centered at 28 kT. Our theoretical results are accompanied by experimental data of QO on a multigrain sodium sample at $T = 0.3$ K and $B_{max} = 18$ T exhibiting a sharp peak at 28 kT, independent of the sample orientation. The persistence of this peak even in the presence of the structural transitions has an implication for using the quantum oscillations of polycrystalline sodium for high magnetic field calibration.

DOI: 10.1103/PhysRevB.101.220103

I. INTRODUCTION

The light alkali elements have a simple electronic structure and are considered ideal elements to study the character and nature of metals [1–9]. All alkali metals adopt a simple bcc structure and a nearly perfect spherical Fermi surface at ambient pressure and temperature. However, at low temperature, the lightest alkalis (Li and Na) undergo martensitic transitions to structures with larger unit cells. Attempts to determine the ground and near ground state structures of these elements have been made for decades, but determination of the crystal structure of the martensite phase in these low-Z elements is challenging because the transitions are incomplete. In lithium, only recently did a combination of experimental and theoretical studies [10,11] based on both crystal and electronic structure succeed in shedding more definitive light on its low-temperature structures.

A martensitic transition directly distorts the nearly spherical Fermi surface. However, most of the experimental and theoretical studies on Na have been focused on the Fermi surface in the bcc phase, and there is very little known about the Fermi surface of the martensite phase. Although experimental observation of quantum oscillation (QO) in the presence of mixed phases is difficult due to phase smearing, each structure has a unique Fermi surface that impacts the overall electronic properties of the sample. Therefore, examination of the Fermi surface of low-temperature Na metal is of basic and fundamental interest.

In fermiology experiments, metals subjected to intense magnetic fields at low temperature exhibit oscillating conductivity and magnetization when the strength of the magnetic field is varied. These effects are known as Shubnikov–de Haas (SdH) and de Haas–van Alphen (dHvA) with regard to oscillating conductivity and magnetization, respectively. In practice, these oscillations are observed by plotting conductivity/magnetization versus 1/B, where B is

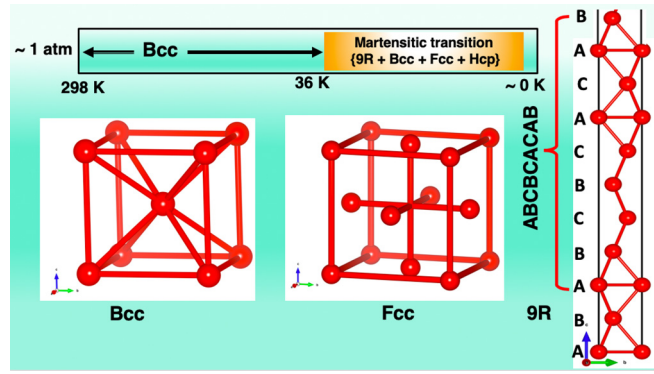

FIG. 1. The bcc, fcc, and 9R structures of sodium at 1 atmosphere pressure.

*se336@cornell.edu
†bonev@llnl.gov
‡deemyad@physics.utah.edu

the applied magnetic field. The SdH/dHvA frequency, f, measured in units of the magnetic field (T or kT in SI), is directly proportional the extremal cross-sectional area A of the Fermi surface perpendicular to **B** as $f = \hbar c/2\pi eA$. Thus, fermiology experiments can be used to determine the geometry of the metal's Fermi surface [12].

In this work, we calculate the Fermi surface of Na for different proposed structures, and compare the results with previously reported data, as well as new measurements of the Fermi surface in a polycrystalline Na sample via SdH oscillations in high magnetic field up to 18 T.

The first observation of the martensitic transition in Na was made by Barrett [13] below 36 K at 1 atmosphere pressure (Fig. 1). Barrett reported a partial martensitic phase transition from a bcc lattice to a distorted bcc structure with small inclusions of a hexagonal-close-packed (hcp) material. The absence of reflection from the [200] plane was the main reason behind Barrett's suggestion that the transition is due to stacking faults of an hcp phase rather than fcc. Later, Perz and Shoenberg [14] suggested that a martensitic transition in Na can be inhibited by careful sample preparation, to obtain high-quality bcc single crystal data at temperatures below 36 K. They also indicated that temperature fluctuations about 36 K can induce martensitic transformation of the sodium crystals. Overhauser [15] proposed a 9*R* stacking fault as the structure of lithium below the martensitic transition. The low-temperature structure of sodium was also proposed to be 9*R*, with stacking sequence *ABCBCACAB* [16].

Early studies showed that despite similarities between electronic properties of Li and Na, the martensitic transition in Na is suppressed by application of high pressure. The combination of theory and experiment explained that in lithium under pressure, the Fermi level gets close to the singular points of the band structure. This effect is absent in Na [17]. Berliner *et al.* [18] proposed that the low-temperature structure of metallic Na is a complex mixture of rhombohedral polytypes, forming a ladder of structures related by a specific stacking fault. Based on crystallography data they interpreted the mixed phases in terms of 9*R*, 15*R*, and 45*R* (long period) almost-hexagonal polytypes or in terms of a two-component 9*R* and 27*R* model. Schwarz *et al.* [19] showed the presence of two long-range-ordered, but faulted, hcp and 9*R* structures. They observed that the measured temperature behavior of Na indicates a higher stability of cubic stacking faults at lower temperatures. Elliott and Datars tried to experimentally study the Fermi surface of sodium with de Haas–van Alphen experiments [20]. After a number of cycles, the dHvA signal dropped below the noise level, which they interpreted as complete martensitic transformation leading to phase smearing and disappearance of QO.

With technological advances in high magnetic field experiments, it is now possible to reach higher magnetic fields with better homogeneity and observe QO even in polycrystalline samples. In previous work, Elatresh *et al.* [11] showed that the measurement of the Li Fermi surface, when compared to first-principles calculations, can be used to detect structural phase transitions and even discriminate between the relevant Li structures at ambient pressure. The approach attempts to circumvent both theoretical and experimental difficulties of standard crystallographic methods and is based on the observation that phase transitions between relevant structures are accompanied by measurable deformations of their Fermi surfaces. In the present work we report a similar analysis for Na and carry out QO measurements on polycrystalline samples. The results from this study can be used to guide and benchmark both future experiments and computations aimed at investigating the Na phase diagram.

II. METHODS

A. Computational methods

All Na structures: bcc, fcc, hcp, and 9*R*, were initially geometrically optimized and then their electronic band structures and Fermi surfaces were calculated using the ABINIT code [21]. In this, we used a nine-electron norm-conserving pseudopotential [22] and the Perdew-Burke- Ernzerhof generalized gradient approximation [23]. The calculations were performed with a 50 Ha energy cutoff and the following converged **k**-point grids for the self-consistent calculations: $46 \times 46 \times 46$ for bcc and fcc; and $32 \times 32 \times 32$ for hcp and 9*R*. These **k**-point meshes ensure convergence of enthalpies to better than 1 meV/atom.

For the electronic properties, non-self-consistent calculations were performed using denser **k**-point grids, namely, $66 \times 66 \times 66$ for bcc and fcc; and $46 \times 46 \times 46$ for hcp and 9*R*.

The Fermi surfaces were calculated with the ABINIT code in a (BXSF) format that can be read by the XCRYSDEN [24] code. The BXSF files specify band energies on a three-dimensional grid within a parallelepiped reciprocal unit cell. We used the Supercell K-space Extremal Area Finder (SKEAF) [25] package to extract all extremal electron/hole Fermi surface orbits. The SKEAF program constructs a large **k**-space "super cell," and uses this to determine quantum oscillation (dHvA/SdH) frequencies, band masses, orbit types (electron or hole), local Fermi surface curvatures, and band density of states contributions.

B. Experimental methods

QO measurements were performed using the SdH effect on multigrain crystals of sodium at ambient pressure at 340 mK and magnetic fields up to 18 T using radio frequency impedance measurements using a tunnel-diode oscillator (TDO) technique [26,27]. This method measures electrical resistance without electrically contacting the sample. For alkalis which are very ductile and chemically reactive, the placement of electrodes distorts the structure and may cause chemical impurities as well. TDO measurements circumvent any potential error caused by placing contact leads on the sample.

C. Analysis

At the National High Magnetic Laboratory (NHMFL), the change of resistivity of Na results from intersections of Landau levels with the Fermi surface as magnetic field is swept. The oscillation of the resistivity is periodic with respect to the inverse of the magnetic field [12]. The magnetic field data collected from NHMFL was not equally spaced. Therefore, a

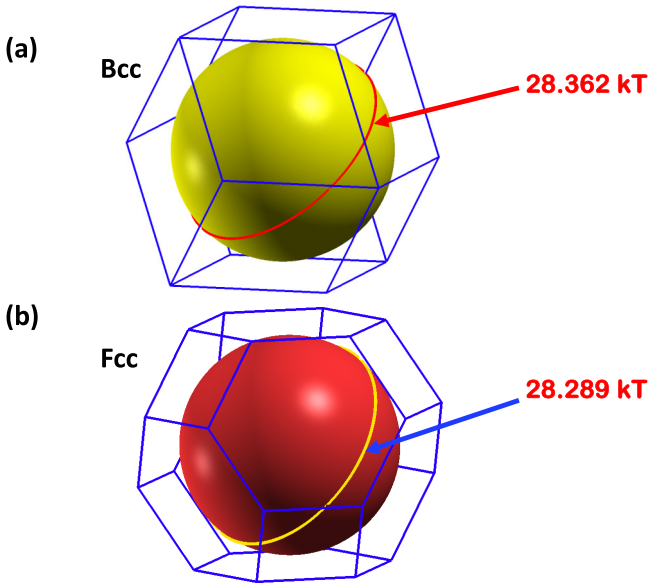

FIG. 2. Brillioun zones, Fermi surfaces, extremal orbits, and dHvA/SdH frequencies for (a) bcc and (b) fcc Na computed for 0 K at 1 atmosphere pressure.

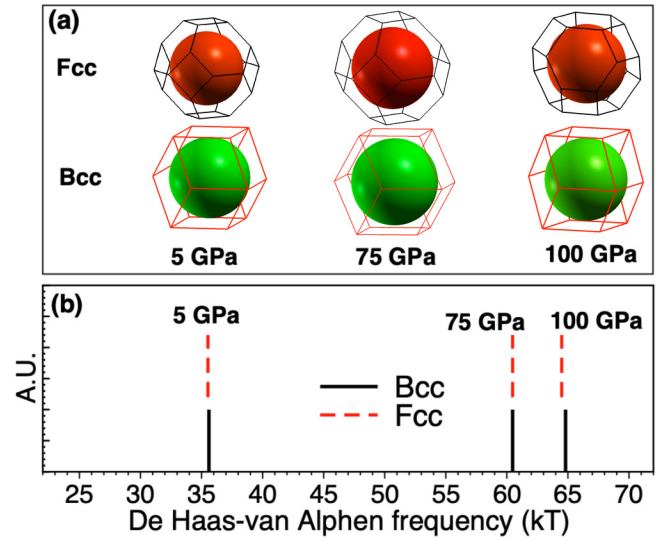

FIG. 3. Fermi surface calculations for bcc and fcc Na computed at 5 and 75 GPa. (a) Brillouin zone and Fermi surface and (b) the dHvA/SdH frequencies for the magnetic field orientations ($\theta = 0$ and $\phi = 0$).

fast Fourier transform (FFT) could not be used to resolve the frequency of oscillations. To find the frequency spectrum, the Lomb-Scargle method was used. It is a least-square method that fits sinusoids to each frequency candidate [28].

III. RESULTS

FS analysis

The calculated FSs of the bcc and fcc Na structures at 1 atmosphere pressure are shown in Fig. 2. In both cases, the FS is nearly perfectly spherical. This is unlike the case of Li, where at the same conditions the fcc FS is slightly deformed and has small necks crossing the Brillouin zone (BZ) boundaries. The computed lattice parameters of the bcc and fcc Na structures are given (see Supplemental Material Table S1 [29]). The computed lattice of the bcc Na structure is $a_0 = 4.198\,45$ Å, which is consistent with the lattice constant measurements of Barrett ($a_0 = 4.225 \pm 0.001$ Å at 1 atmosphere and 5 K) [13] and ($a_0 = 4.2098 \pm 0.004$ Å at 0.3 GPa and 20 K) [30]. The computed FS, band structures, and electronic density of states (see Supplemental Material Figs. S1 and S2 [29]) indicate that bcc and fcc Na are both nearly perfect free-electron metals.

The band structure of the fcc phase at the L symmetry point (see Supplemental Material Fig. S2 [29]) is above the Fermi level and thus is not sufficient to cause a noticeable deformation of the FS or the appearance of necks at the BZ boundaries as in fcc Li [11]. There is a single QO frequency associated with each of these structures, regardless of the crystal orientation relative to the magnetic field. Their calculated values are 28.362 and 28.289 kT for bcc and fcc Na at 1 atmosphere, respectively. According to our calculations, the FS of Na is very slightly deformed in the bcc and fcc structures at 1 atmosphere. The minimum and maximum dHvA/SdH frequencies are 28.361 and 28.381 kT for bcc and 28.2885 and 28.3176 kT for fcc at 1 atmosphere. The corresponding values for $(\max - \min)/(\max + \min)/2$ are just 0.07% and 0.1%. Accurate discrimination of these two frequencies was beyond the capability of this experiment. In contrast to Li, fermiology experiments on Na were not helpful in discriminating between bcc and fcc at 1 atmosphere.

Although Na and Li share a very similar sequence of structural phase transitions in their P-T phase diagrams, the boundaries of these structures as a function of pressure and temperature are vastly different [4,6,10,31]. For example, at 1 atmosphere pressure and room temperature, the bcc structure in Na remains stable up to ~65 GPa, which is ten times higher than the bcc-fcc boundary in Li. The fcc structure of Na extends to pressures as high as ~105 GPa, which is three times higher than that of lithium. The fcc structure in lithium is predicted to show nesting [32], which is suggested to be related to the emergence of pressure-induced superconductivity.

We calculated the shift in the dHvA/SdH frequencies for the bcc vs fcc structures in Na at higher pressures. Figure 3(b) shows a calculated shift in the dHvA/SdH frequencies of Na at 5 and 75 GPa. It is notable that despite the large change of pressure, the FS of Na remains nearly spherical [Fig. 3(a)]. The FS calculations for fcc Na show no evidence of nesting that can be observed up to 100 GPa. Moreover, the FS of both fcc and bcc structures remain nearly identical at comparable pressures. This is consistent with previous calculations [34]. Unlike other alkali metals, Na sustains simple metal behavior to such high pressures and can be used as a standard material representing free-electron behavior in high-pressure experiments.

In the hcp structure, which has a diatomic primitive cell, there are two electronic bands, Nos. 9 and 10, crossing the Fermi level. The FS of these bands and the characteristics of some of their extremal orbits are shown in Fig. 4. While the FS of band 9 has an orbit with QO frequency of 28.277 kT, which is similar to bcc and fcc, both hcp Fermi surfaces exhibit a wide range of frequencies otherwise. The band 9 FS produces

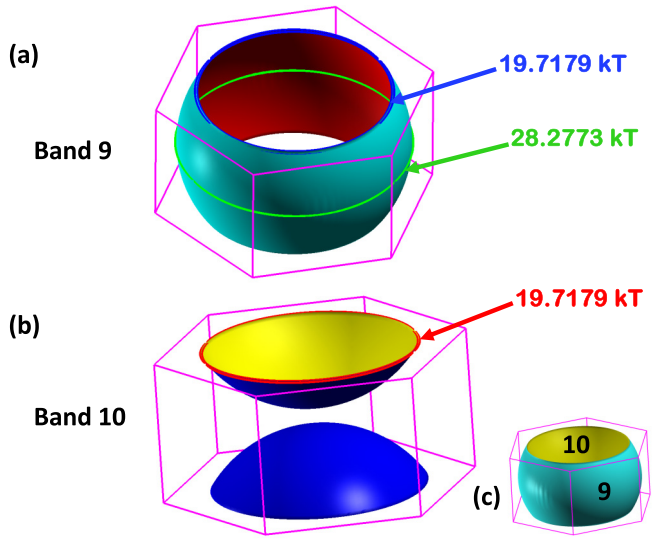

FIG. 4. Brillouin zones, Fermi surfaces, selected extremal orbits, and dHvA/SdH frequencies for hcp Na at 0 K and 1 atmosphere computed for crystal orientations relative to the magnetic field specified by ($\phi = 0^\circ$ and $\theta = 0^\circ$). The definitions of these angles are shown in Fig. S5. Here (a) and (b) show the Fermi surfaces of bands 9 and 10, respectively. The hcp band structure is shown in Fig. S3. The combined FSs of all bands are shown in (c).

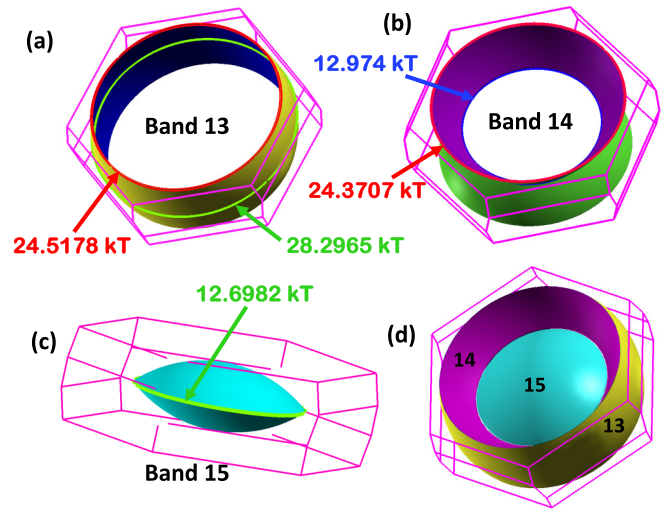

FIG. 5. Brillouin zones, Fermi surfaces, selected extremal orbits, and dHvA/SdH frequencies for 9*R* Na at 0 K and 1 atmosphere computed for crystal orientations relative to the magnetic field specified by ($\phi = 0^\circ$ and $\theta = 0^\circ$). Here (a), (b), and (c) show the surfaces originating from bands 13, 14, and 15, respectively. The 9*R* band structure is shown in Fig. S4. The combined FSs of all bands are shown in (d).

most of the higher QO frequencies (>19.7 kT), while band 10 is responsible for the lower frequencies. Therefore, while the main QO frequency at ∼28 kT will persist in this phase, additional QO peaks will be present in the hcp structure that would allow an experimental detection/measurement of this structure.

The FS of the 9*R* structure, which is the main proposed structure for the low-temperature phase of Na at 1 atmosphere pressure, is shown in Fig. 5. There are three electron bands crossing the Fermi level in 9*R*: bands number 13, 14, and 15, as a result of which the FS here is more complicated, consisting of three separate pieces. Band 15 FS is responsible for a large part of the low QO frequencies, including a cluster of orbits with frequencies around 5 kT. Bands 13 and 14 FS result in a wide range of higher dHvA/SdH frequencies. Again, we observe orbits corresponding to 28.296 kT, which are similar to the characteristicbcc and fcc frequencies and have the largest overall contribution. Nevertheless, the range of QO frequencies and the characteristic low-frequency orbits make 9*R* distinguishable from the other structures when high-resolution measurements are available.

In most fermiology studies, single crystals have an orientation-dependent feature (e.g., H_c or magnetic transition) which can be optimized, and therefore the orientation of the sample can be determined. However, in fermiology measurements at high pressure, one may work with polycrystalline/multigrain samples or the orientation of the crystal may be difficult to determine. Furthermore, even in some ambient pressure measurements, temperature-induced disorder and mixture of several phases may be present in the samples. In order to better relate the theoretical results to potential experimental data, we have calculated the QO frequencies of all possible crystalline orientations for all crystal structure considered. In particular, the data were collected in bin sizes of 0.05 kT, and the orientation of the magnetic field with respect to the respective BZs was varied so that the QO calculations were performed in increments of 1° from 0° to 90° for θ and from 0° to 360° for ϕ. A normalized plot of these frequencies (histogram) represents the spectrum that one would observe in an anisotropic polycrystalline sample. The results are shown in Fig. 6. Additionally, they provide a comparison between the QO frequency spectrum of the four Na structures considered.

Despite similarities between the FS of Li and Na at ambient pressure, lithium exhibits deformations from a perfectly spherical FS. Most significantly, the 42 kT "belly" orbit quickly shifts or disappears for all other low-temperature structures other than and bcc. In the case of Na, the calculated QO for all low-temperature structures persistently contains the "belly" orbit around 28 kT. In pulsed magnetic field, where the detection of NMR is challenging, the Fermi surface of polycrystalline copper has been used to calibrate the high magnetic field. While Cu has a complex and orientation-dependent FS, the robustness of the 28 kT band in Na for all low-temperature structures presents an opportunity to use Na as a standard for calibration in pulsed magnetic field, both at ambient and very high pressures. This is especially effective since the simple method of sample preparation that we used here eliminates the challenges due to high reactivity of Na [34]. The robustness of this band in Na for all low-temperature structures presents an opportunity to use Na as a standard for calibration of high magnetic fields [34].

We attempted to experimentally measure the QO of polycrystalline sodium at low temperature via the detection of SdH oscillations. To minimize the stress introduced by electrical

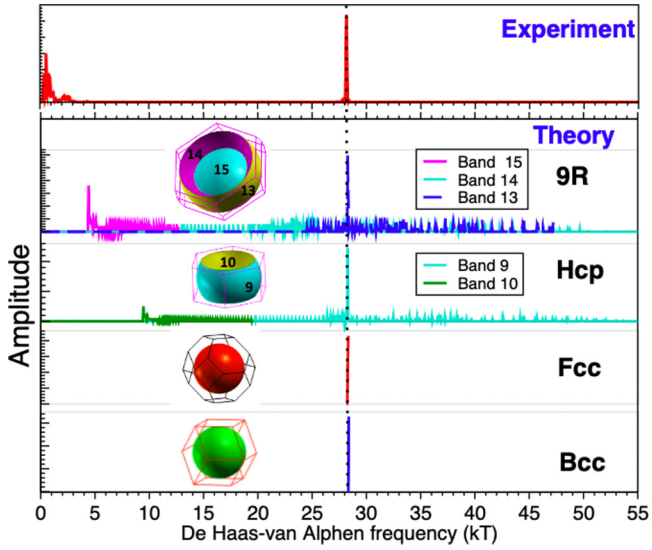

FIG. 6. Spectrum of the dHvA/SdH frequencies for all magnetic field orientations for the Na structures: bcc, fcc, hcp, and 9*R*. The dHvA/SdH frequencies are collected in uniform bin sizes equal to 0.05 kT. All magnetic orientations are considered by varying the angles θ and ϕ from 0° to 360° and 90°, respectively, in increments of 1°. The experimental data were collected at temperature 350 mK using magnetic fields between 16 and 18 T. The dotted vertical line in the figure is a guide for the eye. The Na samples were cut from a high-purity reagent grade dry Na (Sigma-Aldrich) and were embedded.

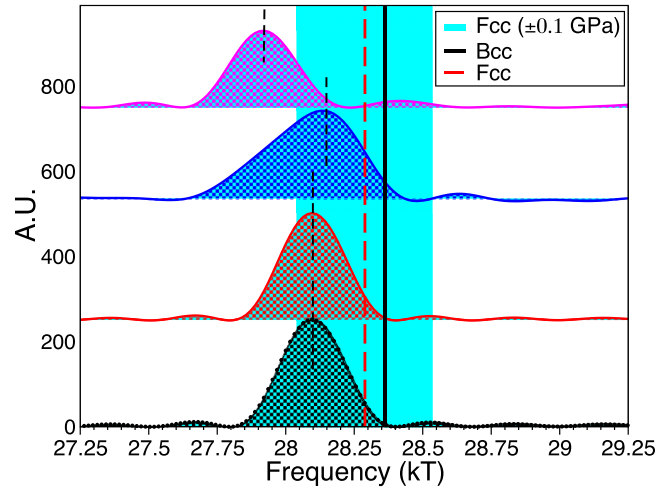

FIG. 7. Fourier spectrum of measured oscillations at four different sample orientations. The short vertical dashed lines indicate the peak positions of the distributions. The long vertical lines (solid and dashed) are the computed frequencies for bcc and fcc at 1 atmosphere pressure, as indicated in the legend. The blue shaded region indicates the variation of the fcc frequency when the pressure is varied by ±0.1 GPa.

contacts on very soft and malleable Na samples, we used the noncontact method based on a tunnel diode oscillator. Since Na is highly reactive with air, we prepared the samples of sodium in molten paraffin wax inside a high-purity argon glovebox. The samples were covered fully by paraffin and remained stable outside of the glovebox for a long period of time. SdH data was collected from the Na samples by sweeping between 15 and 18 T at 0.3 K. The samples were slowly cooled down at (<0.3 K/min), and the SdH data were collected at 0.3 K by sweeping the magnetic field between 15 and 18 T at 0.15 T/min. We did not detect any noticeable change in the QO of the sample as a function of time for the duration of the experiments that lasted more than 48 h. To ensure that we detect all the possible oscillations from every crystal orientation, we rotated the sample in small intervals between 0° and 90°. We note the good agreement between the observed fermiology measurement with the calculated frequencies, Fig. 6, which further validates our approach. The measured frequency is indistinguishable from the calculated values around 28 kT for bcc and fcc. From this comparison, we can conclude the experimental Na sample contained one or both of these structures.

IV. DISCUSSION

In this work we provide a theoretical analysis along with fermiology measurement for Na at 1 atmosphere which can be used as guidance for future theoretical and experimental work.

It has been previously reported that repeated temperature cycling above and below 36 K has an important influence and could induce complete or partial martensitic transformation of sodium [14]. In fact, Elliott and Datars interpreted the drop in the amplitude of the quantum oscillations signal after some temperature cycling as due to an essentially complete martensitic transformation. They even stated that "Further temperature cycling did not restore the signal amplitude (17). By taking advantage of more homogeneous and higher magnetic fields that are currently accessible, we could revisit these measurements and perform fermiology measurements on multigrain sodium samples at 1 atmosphere.

Figure 7 shows selected FFT analysis of the background-subtracted data of TDO frequency vs inverse magnetic field offset for clarity at different angles. The QO of the same Na sample is plotted at four different orientations. All data points show a distinct persistent frequency of the large peak around 28 kT with a small shift (Fig. 7). This shift is less than 0.2 kT, and the average frequency of these peaks is ∼28.06 kT. To estimate how sensitive the SdH frequencies are to variations of the lattice parameters, we have calculated the frequency of the fcc structure at 0.1 GPa. The lattice parameters in our calculations at 0 and 0.1 GPa are given in Supplemental Material Table S1 [29]. Figure 7 shows the shift in frequency in fcc due to changing the pressure by 0.1 GPa, which corresponded with 0.55% change in lattice parameter (see Supplemental Material Table S1 [29]).

In Figure 8, we plot a histogram of the peak frequencies observed for all measured angles. It is clear that only two very close frequencies are present, which may originate from two of the low-temperature structures present in Na. We did not detect any other lower or higher frequency oscillations. The slight shift in the observed frequencies together with the extremely simple Fermi surface make Na an excellent material to be used for calibration standard in high magnetic field

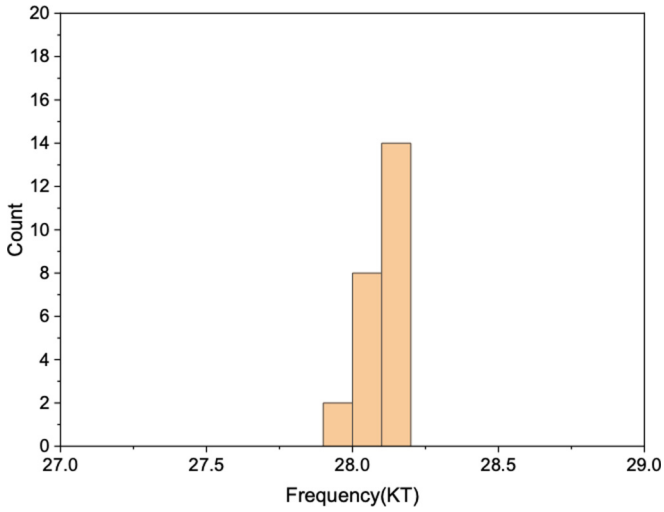

FIG. 8. A histogram analysis of the peaks frequencies observed in fermiology measurement for all the measured orientations (see Supplemental Material for Fourier spectra of the sample at all orientations [29]).

measurements in the largest pressure range for any metal up to 100 GPa.

In summary, we have performed first-principles calculations based on density functional theory combined with fermiology measurement. We have achieved an excellent agreement between our experimental data and theory, showing that independent of the time or temperature cycling or orientation of the sample, a strong and narrow peak was present at 28 kT. We suggest that Na can be used as a standard sample for the high magnetic field measurements.

ACKNOWLEDGMENTS

S.F.E. thanks Elisabeth J. Nicol for the research support and discussion. The theoretical work was supported by the Energy Frontier Research in Extreme Environments (EFree) Center, an Energy Frontier Research Center funded by the US Department of Energy, Office of Science under Award No. DE-SC0001057, and by LLNL. The work at LLNL was performed under the auspices of the US DOE under Contract No. DE-AC52-07NA27344. The experimental research at University of Utah was supported by National Science Foundation-Division of Materials Research Award No. 1351986 and the US Department of Energy, Office of Science, Fusion Energy Sciences under Award No. DE-SC0020340. The National High Magnetic Field Laboratory is supported by the National Science Foundation through NSF/DMR-1157490/1644779 and the State of Florida. The work at NHMFL was also partially funded by the US DOE under NNSA SSAA DE-NA0001979.

S.F.E., S.A.B., S.D., and R.H. designed the research. S.F.E. performed the theoretical calculations. S.A.B., N.W.A., and R.H. supervised the theoretical research. A.D.G., W.A.C., and S.W.T. provided user support for the magnet time. Experimental data collection, analysis, and sample preparation were performed by M.T.H., T.B., A.D.G., W.C., and S.D. S.D. designed and supervised the experiments. All authors contributed to the writing of the paper.

[1] J. B. Neaton and N. W. Ashcroft, Nature (London) **400**, 141 (1999).
[2] J.-Y. Raty, E. Schwegler, and S. A. Bonev, Nature (London) **449**, 448 (2007).
[3] N. W. Ashcroft, Phys. Rev. B **39**, 10552 (1989).
[4] C. L. Guillaume, E. Gregoryanz, O. Degtyareva, M. I. McMahon, M. Hanfland, S. Evans, M. Guthrie, S. V. Sinogeikin, and H.-K. Mao, Nat. Phys. **7**, 211 (2011).
[5] J. Tuoriniemi, K. Juntunen-Nurmilaukas, J. Uusvuori, E. Pentti, A. Salmela, and A. Sebedash, Nature (London) **447**, 187 (2007).
[6] F. A. Gorelli, S. F. Elatresh, C. L. Guillaume, M. Marqués, G. J. Ackland, M. Santoro, S. A. Bonev, and E. Gregoryanz, Phys. Rev. Lett. **108**, 055501 (2012).
[7] A. M. Schaeffer, W. Cai, E. Olejnik, J. J. Molaison, S. Sinogeikin, A. M. dos Santos, and S. Deemyad, Nat. Commun. **6**, 8030 EP (2015).
[8] S. F. Elatresh, S. A. Bonev, E. Gregoryanz, and N. W. Ashcroft, Phys. Rev. B **94**, 104107 (2016).
[9] S. F. Elatresh, Z. Zhou, N. W. Ashcroft, S. A. Bonev, J. Feng, and R. Hoffmann, Phys. Rev. Mater. **3**, 044203 (2019).
[10] G. J. Ackland, M. Dunuwille, M. Martinez-Canales, I. Loa, R. Zhang, S. Sinogeikin, W. Cai, and S. Deemyad, Science **356**, 1254 (2017).
[11] S. F. Elatresh, W. Cai, N. W. Ashcroft, R. Hoffmann, S. Deemyad, and S. A. Bonev, Proc. Natl. Acad. Sci. USA **114**, 5389 (2017).
[12] D. Shoenberg, *Magnetic Oscillations in Metals* (Cambridge University Press, Cambridge, 2009).
[13] C. S. Barrett, Acta Crystallogr. **9**, 671 (1956).
[14] J. M. Perz and D. Shoenberg, J. Low Temp. Phys. **25**, 275 (1976).
[15] A. W. Overhauser, Phys. Rev. Lett. **53**, 64 (1984).
[16] R. Berliner, O. Fajen, H. G. Smith, and R. L. Hitterman, Phys. Rev. B **40**, 12086 (1989).
[17] V. G. Vaks, M. I. Katsnelson, V. G. Koreshkov, A. I. Likhtenstein, O. E. Parfenov, V. F. Skok, V. A. Sukhoparov, A. V. Trefilov, and A. A. Chernyshov, J. Phys.: Condens. Matter **1**, 5319 (1989).
[18] R. Berliner, H. G. Smith, J. R. D. Copley, and J. Trivisonno, Phys. Rev. B **46**, 14436 (1992).
[19] W. Schwarz, O. Blaschko, and I. Gorgas, Phys. Rev. B **46**, 14448 (1992).
[20] M. Elliott and W. R. Datars, J. Phys. F: Me.tal Phys. **12**, 465 (1982).
[21] X. Gonze, B. Amadon, P.-M. Anglade, J.-M. Beuken, F. Bottin, P. Boulanger, F. Bruneval, D. Caliste, R. Caracas, M. Côté *et al.*, Comput. Phys. Commun. **180**, 2582 (2009).
[22] M. van Setten, M. Giantomassi, E. Bousquet, M. Verstraete, D. Hamann, X. Gonze, and G.-M. Rignanese, Comput. Phys. Commun. **226**, 39 (2018).
[23] J. P. Perdew, K. Burke, and M. Ernzerhof, Phys. Rev. Lett. **77**, 3865 (1996).

[24] A. Kokalj, Comput. Mater. Sci. **28**, 155 (2003).
[25] P. Rourke and S. Julian, Comput. Phys. Commun. **183**, 324 (2012).
[26] W. A. Coniglio, L. E. Winter, C. Rea, K. Cho, and C. C. Agosta, Improvements to the tunnel diode oscillator technique for high frequencies and pulsed magnetic fields with digital acquisition, arXiv:1003.5233.
[27] C. T. Van Degrift, Rev. Sci. Instrum. **46**, 599 (1975).
[28] J. T. VanderPlas, Astrophys. J. Suppl. Ser. **236**, 16 (2018).
[29] See Supplemental Material at http://link.aps.org/supplemental/10.1103/PhysRevB.101.220103 for theoretical and experimental data analysis.
[30] W. Cai, M. T. Hossain, J. Coles, J. Lybarger, J. Blanton, E. Sterer, and S. Deemyad, High Press. Res. **39**, 628 (2019).
[31] M. I. McMahon, E. Gregoryanz, L. F. Lundegaard, I. Loa, C. Guillaume, R. J. Nelmes, A. K. Kleppe, M. Amboage, H. Wilhelm, and A. P. Jephcoat, Proc. Natl. Acad. Sci. USA **104**, 17297 (2007).
[32] D. Kasinathan, J. Kuneš, A. Lazicki, H. Rosner, C. S. Yoo, R. T. Scalettar, and W. E. Pickett, Phys. Rev. Lett. **96**, 047004 (2006).
[33] R. Tutchton, X. Chen, and Z. Wu, J. Chem. Phys. **146**, 014705 (2017).
[34] W. A. Coniglio, A. F. Williams, A. Yannakopoulos, A. Grockowiak, and S. Tozer, *APS March Meeting Abstracts* (APS, 2016), p. V46.007.